Fully Automated Wide Temperature Range Semiconductor Characterization

Frank S.R., Hansel J., Bitterle J., Schwendemann R., Hiller M.
Karlsruhe Institute of Technology (KIT), Institute of Electrical Engineering (ETI)
Kaiserstraße 12
Karlsruhe, Germany
Tel.: +49 721 608 42465
Email: s.frank@kit.edu

URL: http://www.kit.edu

ACKNOWLEDGMENTS

This work was carried out within the hydrogen flagship project TransHyDE and was funded by the Federal Ministry of Education and Research under the funding grant number 03HY204A. The responsibility for the content of this publication lies with the authors.

***Index Terms*—≪IGBT≫, ≪SiC MOSFET≫, ≪Semiconductor device≫, ≪I-V signature≫, ≪Test bench≫, ≪Double pulse test≫**

***Abstract*—This paper introduces a fully automated test bench for $-75\,^{\circ}\mathrm{C}$ up to $160\,^{\circ}\mathrm{C}$ static and dynamic semiconductor characterization. First measurements performed with a $1.2\,\mathrm{kV}$, $200\,\mathrm{A}$ Si-IGBT module and a $1.2\,\mathrm{kV}$, $250\,\mathrm{A}$ SiC-MOSFET module show better semiconductor performance at lower temperatures compared to the conventional high temperature operation.**

I. INTRODUCTION

Superconducting electrical machines as well as superconducting supply lines are supposed to become a trend in future energy generation and distribution systems [1–5]. In the project associated to [6] a hybrid Liquid Hydrogen (LH2) and High Temperature Superconductor (HTS) supply line is investigated. The applied HTSs need to be operated at very low temperatures that are typically below $77\,\mathrm{K}$ to ensure a safe operation and to enable the necessary critical currents. In case of the LH2-HTS pipeline, even temperatures below $20\,\mathrm{K}$ are necessary to keep the hydrogen in a liquid state. For that reason, a proper cooling at cryogenic temperatures is essential. However, those applications require power electronics, i.e. converters for the grid connection of the hybrid supply line or inverters for the superconducting machine plus for other common auxiliaries such as compressors and pumps.

The very powerful cooling units and the cryogenic temperatures allow an operation of the semiconductors at much lower temperatures than it is common practice. Moreover, the conventional approach to converter design, in which the converter and its cooling are designed in such a way that the semiconductors full load junction temperature is close to its maximum, is no longer required. Instead, a cooling at a much lower temperature gives the opportunity to control the junction temperature in a wider range. This can be used to operate the device at its application specific optimum operating point. For that reason, an investigation of the semiconductors low-temperature behavior is reasonable to identify possible operating points with lower switching and conduction losses that can result in a better power electronics efficiency.

Moreover, for the interface converters of the hybrid supply line the use of topologies with galvanic isolation opens up the possibility to use this isolation also for thermal isolation. This in turn reduces the necessary cooling power and allows a better efficiency of the overall system.

Hence, for an optimized system, good knowledge of the semiconductor behavior over a wide temperature range is required. Therefore, this paper introduces a fully automated semiconductor test bench for dynamic and static characterization. To reduce costs, the number of measuring devices used is kept as low as possible. Thus, the proposed setup for static measurements allows the measuring of the *I-V* curve without additional expensive test equipment such as curve tracers.

This paper is structured into six sections. The second

section gives an overview of recent research on low-temperature semiconductor characterization and the associated challenges. Section III presents a fully automated measurement setup that allows characterization over the wide temperature range from $-75°C$ up to $160°C$. In section IV the control and measurement data evaluation software of the test bench is explained. First measurements are performed with a $1200\,V$, $200\,A$ Si-IGBT module and a $1200\,V$, $250\,A$ Silicon Carbide (SiC)-MOSFET module. The results with a focus on the static behavior are outlined in section V. Finally, the results are discussed and an outlook on future work is given.

II. Low-temperature semiconductor characterization

In recent years, more and more research has been conducted on the low-temperature behavior of power semiconductors. In [7], SiC PIN and Schottky diodes are investigated down to $20\,K$ and in [8] two commercial $1.2\,kV$ SiC-MOSFETs are characterized down to $30\,K$. The authors in [9] and [10] present the static and dynamic characterization of a planar and a trench SiC-MOSFET as well as a Si-IGBT over the wide temperature range from $90\,K$ to $493\,K$. Further cryogenic measurements of three and six different $1.2\,kV$ SiC-MOSFETs are published in [11] and [12], respectively. Whereas in [13], the focus is on the body diode of a $1.2\,kV$ SiC-MOSFET which is investigated from $90\,K$ to $603\,K$. These investigations use liquid nitrogen or liquid helium chillers, causing quite complex and expensive cooling. Moreover, probably due to the circumstance of limited space in the thermal chamber, mostly relatively small discrete semiconductors are investigated with currents $< 80\,A$.

A review on numerous power electronic components as different semiconductors, passive components and interconnections is given in [14], while [15] gives an overview of SiC and Gallium Nitride (GaN) components characteristics at cryogenic temperatures. For temperatures below $250 - 300\,K$ according to [9], [10], [11] and [15] especially the static behavior of SiC components gets worse, while the switching losses show various trends but are not significantly improved in any case. Therefore, for those semiconductors a measurement at cryogenic temperatures is not expedient. In contrast, silicon and GaN components show extensive improvements even at cryogenic temperatures [14], [15].

While previous investigations put a focus on rather small discrete components, the test bench presented here focuses on the characterization of complete semiconductor modules. To keep the cooling effort within limits, a temperature range of $198\,K$–$433\,K$, which corresponds to $-75\,°C$–$160\,°C$, is considered sufficient.

III. Semiconductor Test Bench

To enable safe measurements at temperatures below $0\,°C$, the double pulse test bench introduced in [16] is extended by a low-temperature measurement chamber. This chamber is hermetically sealed. Before each measurement, the chamber is flooded with gaseous nitrogen to minimize humidity and therefore the risk of dew formation and icing inside. A front view of the chambers principle structure is given in Fig. 1a, the real-world setup is pictured in Fig. 1b.

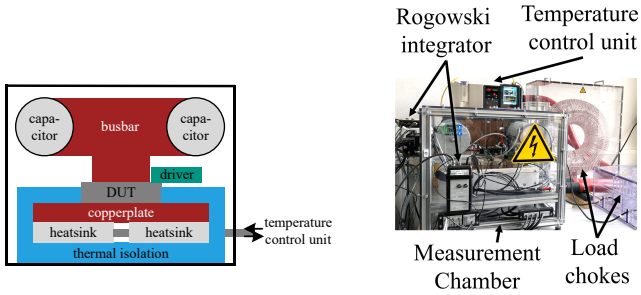

(a) Principal structure (b) Real-world setup

Fig. 1: Low-temperature measurement chamber

The semiconductor module as Device Under Test (DUT) is placed on a copperplate, the temperature of which is regulated using a *HUBER Unistat 815W* temperature control unit. Thermal isolation (cf. Fig. 1a) reduces the heat flow into the DUT and the tempering plate for low-temperature measurements. This allows tempering plate temperatures to reach a minimum of about $-75°C$. The gate drivers, the DC link capacitors, the voltage and current probes as well as the temperature measurement are placed inside the chamber. In contrast, the load choke and temperature sensitive measurement technology such as the Rogowski coil integrator are placed outside. To monitor and supervise the humidity inside, a *Sensirion SHT40* temperature and humidity sensor is installed inside the chamber. The status of the chamber is displayed optically with an RGB-LED.

Beside the temperature of the tempering plate, which is measured by the temperature control unit, the test bench has seven additional temperature channels. Those can be used for measuring and supervising the temperature of certain converter parts, like the gate-drivers, the

internal module temperature, if e.g. an internal temperature sensor is available, or of any passive component or busbar.

For the measurement, the galvanically isolated delta-sigma Analog to Digital Converter (ADC) *AMC3336* from *Texas Instruments* is used in combination with an adaption circuit for the particular used sensor. With a defined temperature range from $-80°\mathrm{C}$ to $200°\mathrm{C}$, a PT100 sensor reaches a resolution of $0.218°\mathrm{C}$. For a PT1000 sensor the resolution can be increased to $0.041°\mathrm{C}$. Additionally, a fixture for an infrared camera allows the supervision of e.g. the temperatures of the gate driver Printed Circuit Board (PCB).

The design of the chamber enables the measurement of various semiconductor modules as well as discrete semiconductors. The latter can be tempered by immersion in an oil pan with the insulating fluid *MiVolt DF7*. The most important technical data of the chamber is summarized in Tab. I.

TABLE I: Technical data of the measurement chamber

Dimensions measurement chamber ($l \times w \times h$)	$58 \times 58 \times 52\,\mathrm{cm}$
Dimensions tempering plate	$32 \times 32\,\mathrm{cm}$
Temperature range tempering plate	$-75°\mathrm{C} - 160°\mathrm{C}$
Internal DC link capacitance	$2.1\,\mathrm{mF}$
Maximum DC link voltage	$1.8\,\mathrm{kV}$

IV. Test Bench Control and Data Evaluation

For a safe, user-friendly and easy control of the test bench, an in-house developed *MATLAB*-based software tool is used. This software sets the measurement and device configuration, controls the measurement as well as evaluates and plots the acquired data from the oscilloscope. The structure of the developed software is depicted in Fig. 2. For the interaction with the user, a *MATLAB* graphical user interface (GUI) is used.

A. Measurement Configuration and Control

In a first step, the measurement is configured by specifying a three-dimensional current, voltage and temperature operating point matrix. Further, important information of the DUT is captured. Thereafter, during device configuration, the parameters of the test bench are defined. This includes the possible temperature and voltage range of the temperature control and power supply unit, as well as oscilloscope parameters like trigger, time and input settings. All settings can be saved in *.json* configuration files, which allows a save and easy reproduction of the settings if several measurements are made.

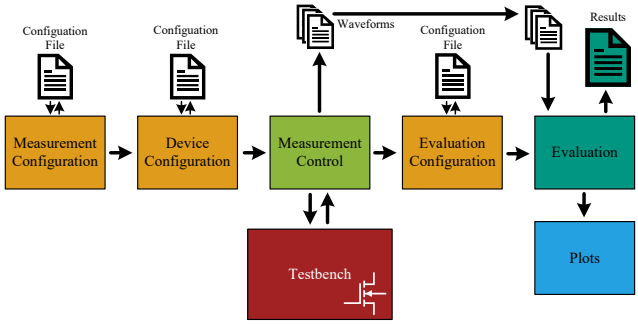

Fig. 2: Software structure of the control and data evaluation software

After configuration, the measurement control performs the automated measurement process, including the communication with the test bench, the setting of the measurement points as well as the reading and saving of the gathered oscilloscope data. Moreover, it supervises the measuring and reacts to possible errors as the opening of the measuring chamber during operation, the pressing of the emergency stop or the loss of test bench communication.

The pulse generation, temperature and humidity sensor readout, test bench supervision and error handling is adopted by an in-house developed signal processing system based on the *Zynq7015* System on Chip (SOC), similar to [17]. A feed-forward control of the DC link voltage is included to calculate its discharge during the first pulse. Furthermore, ahead of each measurement, the energy in the DC link capacitor before the pulse is compared with the energy in the load inductance after the first pulse:

$$\frac{E_\mathrm{C}}{E_\mathrm{L}} = \frac{C \cdot V^2}{L \cdot I^2} \overset{!}{>} 5 \tag{1}$$

Operating points with a proportion lower than five are skipped during the measurement, since otherwise the DC link capacitor would be discharged too much for a reliable measurement. This can be prevented by using a sufficiently large DC link capacitance as well as sufficiently high DC link voltages.

After each measurement, the oscilloscope data are saved together with all currently measured temperatures in a *.json* file. Additionally, this file contains all measurement and device configuration information as well. This ensures an unambiguous assignment of the measurement data, as well as a comparability of different measurements.

B. Measurement Data Evaluation

Within the developed *MATLAB* app, the post-processing for analyzing and evaluating the gathered data is implemented. Several evaluation settings allow a wide range of use. This includes the choice of integral borders for loss calculation, so that these e.g. can be chosen individually for IGBTs or MOSFETs according to [18] and [19]. The evaluation configuration can be saved to a *.json* file and imported again. Fig. 3 shows a flowchart of the detailed evaluation process.

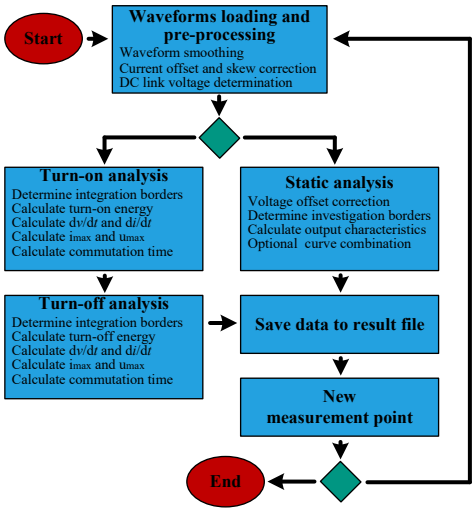

Fig. 3: Evaluation process

During pre-processing, the oscilloscope data is read, offset-adjusted and optionally smoothed. For a reliable switching loss calculation, the skew between the voltage and current waveform caused by different propagation delays due to different probes and cable lengths has to be compensated. According to [20], even a small skew of several nanoseconds can cause huge errors. Skew compensation can be done either by using previous calibration measurements or alternatively, the software can automatically determine the latency between the voltage and current for each measurement. Therefore, during the turn-off process the points in time with the highest rate of current fall and the maximum voltage are determined. Due to

$$v = L \cdot \frac{\mathrm{d}i}{\mathrm{d}t} \tag{2}$$

those two points in time have to be simultaneous. With this information, the skew can be corrected. After pre-processing, depending on the type of investigation, either the turn-on and turn-off energy or the output characteristic are calculated. For dynamic characterization, the software identifies the integration borders according to the users definition as described above and integrates the switching power over time. Beside the turn-on and turn-off losses, other parameters like $\mathrm{d}v/\mathrm{d}t$, $\mathrm{d}i/\mathrm{d}t$, maximum over-current and -voltage or commutation time are calculated. Those can be used for a proper Electromagnetic compatibility (EMC) converter design and for a suitable setting of dead times. The process for static characterization is described in detail in subsection V-B.

V. Measurements

To measure the switching dynamics, the established double pulse setup as described e.g. in [16] and pictured in Fig. 4a can be used. The low-side transistor as DUT is switched. With the first pulse, the desired load current is built up. After a short delay a second pulse can be used to capture the turn-on and turn-off behavior.

In the following, measurement results for the *FF6MR12KM1* SiC-MOSFET and the *FF200R12KE4* Si-IGBT module from *Infineon* are presented.

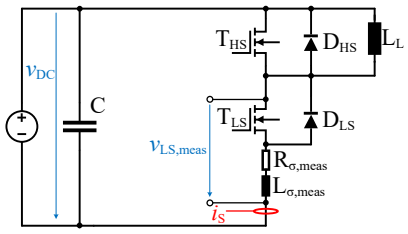

(a) Dynamic measurement

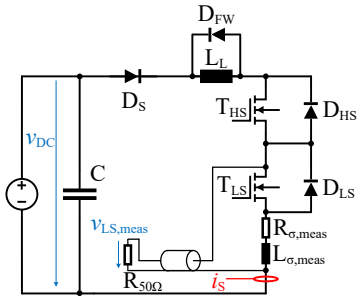

(b) Static measurement

Fig. 4: Test bench setup for dynamic and static characterization

A. Dynamic Characterization

Exemplary waveforms for turn-on and turn-off of the *FF200R12KE4* Si-IGBT module at $V_{\mathrm{CE}} = 600\,\mathrm{V}$, $I_{\mathrm{E}} = 200\,\mathrm{A}$ are shown in Fig. 5. The automatically identified integral borders are printed as vertical lines. The measurement conditions are given in Tab. II in subsection V-C.

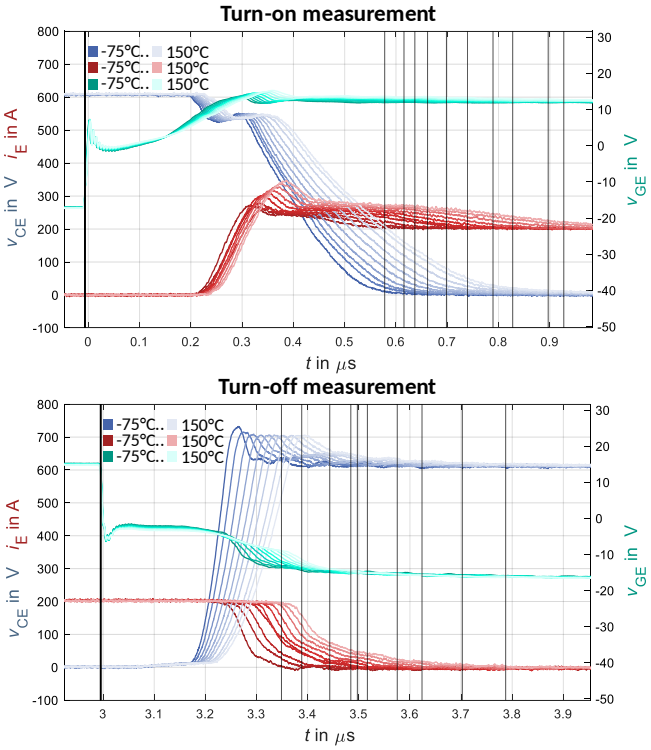

Fig. 5: Exemplary waveforms *FF200R12KE4* Si-IGBT module at $V_{\mathrm{CE}} = 600\,\mathrm{V}$, $I_{\mathrm{E}} = 200\,\mathrm{A}$, $T = -75 - 150\,^{\circ}\mathrm{C}$

By evaluating the waveforms with the software, the dynamic characteristics given in Fig. 6 are obtained. This paper presents the results of the switching characteristics for the Si-IGBT module as an example. As shown, turn-on and turn-off energies can both significantly be reduced for lower temperatures. The overvoltage remains almost constant with a slight increase at temperatures below $-25\,^{\circ}\mathrm{C}$, while the overcurrent rises significantly for higher temperatures.

B. Static Characterization

Theoretically, the dynamic characterization setup can also be used for characterizing the static behavior. Therefore, only the first pulse would be necessary. During the low side transistors on-state the current through and the voltage across this component need to be measured.

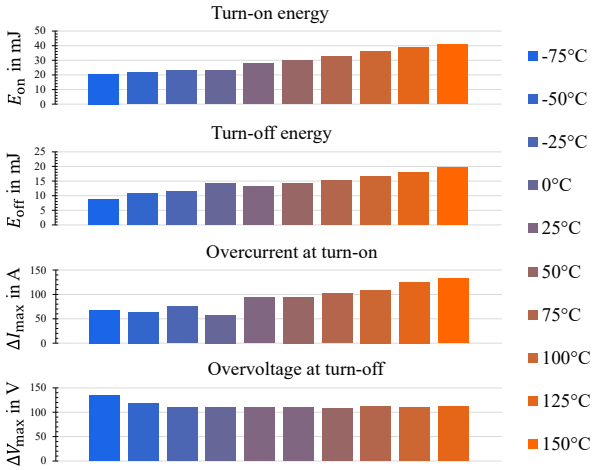

Fig. 6: Dynamic characteristics of the *FF200R12KE4* Si-IGBT module at $V_{\mathrm{CE}} = 600\,\mathrm{V}$, $I_{\mathrm{E}} = 200\,\mathrm{A}$, $T = -75 - 150\,^{\circ}\mathrm{C}$

However, when using this setup for static characterization problems during the measurement acquisition occur. Before the first pulse, when T_{LS} is turned off the voltage across the semiconductor equals the very high DC link voltage in the range of several hundred volt. In contrast to that, the voltage across the transistor during on-state is in the range of a few volts. Hence, for an accurate voltage measurement the oscilloscope range should be a few volts as well. When doing so, due to internal or external voltage clipper circuits, which are then necessary, the oscilloscope needs some time during turn-on to capture the data correctly. Hence, not the complete pulse can be used for evaluation.

Furthermore, to withstand the high voltage during off-state, high voltage probes should be used, which typically have a lower accuracy. To solve that problem, curve tracers as described e.g. in [11] can be used instead of the double pulse setup. However, this requires an additional, quite expensive analyzer. Alternatively, the setup shown in Fig. 4b can be used.

Instead of connecting the choke in parallel to the high-side transistor, it is connected in series together with an additional free-wheeling diode. The voltage across the low-side transistor is measured $1:1$ using a coaxial cable and an external $50\,\Omega$ termination resistor at the oscilloscope input. During the measurement, the low-side transistor is turned on first, while the high-side transistor is still off. Hence, nearly the complete DC link voltage is across the high-side transistor. By turning the high-

side transistor on, a current through the choke and both transistors is built up. In Fig. 7 an exemplary waveform measured at $T = 20°\mathrm{C}$ for the *FF200R12KE4* Si-IGBT module is given. The current i_E and voltage v_CE of the low-side transistor are depicted in red and light-blue, its gate voltage is given in green. The dark-blue waveform represents the DC link voltage v_DC.

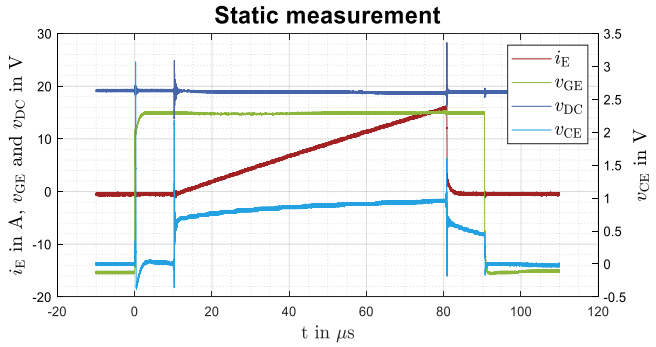

Fig. 7: Exemplary single pulse waveform for static measurement of the *FF200R12KE4* Si-IGBT module at $T = 20°C$

Due to the output capacitances of both transistors and the freewheeling diode as well as the module inductance, during both switching events a short oscillation in the voltage across the low-side transistor occurs, but with its maximum amplitude being lower than $3\,\mathrm{V}$ and its duration lower than $1\,\mu\mathrm{s}$ is not significantly disturbing to the measurement. For higher values of V_DC and i_T up to $250\,\mathrm{V}$ and $500\,\mathrm{A}$, the maximum amplitude value of the oscillation is higher, but stays lower than $40\,\mathrm{V}$ for each investigated operating point.

The inductance $L_{\sigma,\mathrm{meas}}$ and the resistance $R_{\sigma,\mathrm{meas}}$ in the measuring path cause a voltage drop

$$v_{\sigma,\mathrm{meas}} = L_{\sigma,\mathrm{meas}} \cdot \frac{\mathrm{d}i_\mathrm{T}}{\mathrm{d}t} + R_{\sigma,\mathrm{meas}} \cdot i_\mathrm{T}. \tag{3}$$

To properly determine the transistors forward voltage, the voltage $v_{\sigma,\mathrm{meas}}$ has to be calculated. For its inductive part, two waveforms with different DC link voltages, resulting in two different rates of current rise $\frac{\mathrm{d}i_\mathrm{T}}{\mathrm{d}t}|_{V_\mathrm{DC,1}}$ and $\frac{\mathrm{d}i_\mathrm{T}}{\mathrm{d}t}|_{V_\mathrm{DC,2}}$, are measured. By inserting both current rates into eq. (3) and calculating the difference for a common absolute current value, the inductance $L_{\sigma,\mathrm{meas}}$ can be calculated:

$$L_{\sigma,\mathrm{meas}} = \frac{v_{\sigma,\mathrm{meas},2} - v_{\sigma,\mathrm{meas},1}}{\frac{\mathrm{d}i_\mathrm{T}}{\mathrm{d}t}|_{V_\mathrm{DC,2}} - \frac{\mathrm{d}i_\mathrm{T}}{\mathrm{d}t}|_{V_\mathrm{DC,1}}} \tag{4}$$

Note, that due to the present design of the measuring circuit this inductance consists of the internal module and external busbar inductance (cf. Fig. 8). However, by redesigning the setup and placing a voltage probe directly at the module terminals, this setup could be used for module inductance measurements as well. To calculated the rate of current rise, the applied DC link voltage V_DC and the inductance of the load choke L_L are used:

$$\frac{\mathrm{d}i_\mathrm{T}}{\mathrm{d}t} = \frac{V_\mathrm{DC}}{L_\mathrm{L}} \tag{5}$$

Here, an ideal load choke and a constant DC link voltage are assumed, which is valid as a first approximation, but has to be verified for each operating point and measurement setup.

The resistance $R_{\sigma,\mathrm{meas}}$, primarily consisting of the PCBs track resistance and the contact resistance between the PCB and the module, was measured to approximately $90\,\mu\Omega$. With a maximum current of $500\,\mathrm{A}$ this would result in a maximum error of around $45\,\mathrm{mV}$. With the gathered information, the software automatically calculates and corrects the influence of $v_{\sigma,\mathrm{meas}}$.

C. Wide Temperature Range Output Characteristics

The setup described in subsection V-B is used to measure the output characteristics of the two modules mentioned above. The measurement conditions are summarized in Tab. II

TABLE II: Measurement conditions

Temperature range	$-75 - 150°\mathrm{C}$
DC link voltage	$20 - 250\,\mathrm{V}$ (static), $600\,\mathrm{V}$ (dynamic)
Max. current	$400\,\mathrm{A}$ (IGBT), $475\,\mathrm{A}$ (SiC-MOSFET)
V_GE / V_GS	$-15/15\,\mathrm{V}$ (IGBT), $-5/15\,\mathrm{V}$ (SiC-MOSFET)
Ext. gate resistor $R_{\mathrm{G,on}}$	$2.7\,\Omega$ (IGBT), $3\,\Omega$ (SiC-MOSFET)
Ext. gate resistor $R_{\mathrm{G,off}}$	$2.7\,\Omega$ (IGBT), $3.9\,\Omega$ (SiC-MOSFET)
DC link capacitance	$2.1\,\mathrm{mF}$ sec. chamber cap. (static) $125\,\mu\mathrm{F} + 2.1\,\mathrm{mF}$ (dynamic)
Inductance load choke	$71.4\,\mu\mathrm{H}$ (static), $349\,\mu\mathrm{H}$ (dynamic)
Oscilloscope	*Lecroy HDO 4104*, $1\,\mathrm{GHz}$, $12\,\mathrm{bit}$
Current probe	*CWT UltraMini CWTUM/3/R*
Voltage probe	Direct coaxial cable 1:1 (static), PPE 4kV (dynamic)

It is important to consider the self-heating of the chip while ramping up the current. Therefore, the load inductance should not be chosen too large to reduce the pulse length and thus the current time area of the transistors current. Hence, especially for the static measurements which were performed with quite low DC link voltages up to $250\,\mathrm{V}$, a lower inductance of $71.4\,\mu\mathrm{H}$ is

used. Previous simulations with the thermal data given in the data sheets [21] and [22] show a maximum junction temperature increase smaller than 5 K for all investigated operating points with the measurement conditions given in Tab. II.

In Fig. 8 the setup for a measurement at $-75°C$ is shown. Only a negligible amount of ice at the connection screws and on the tempering plate is visible.

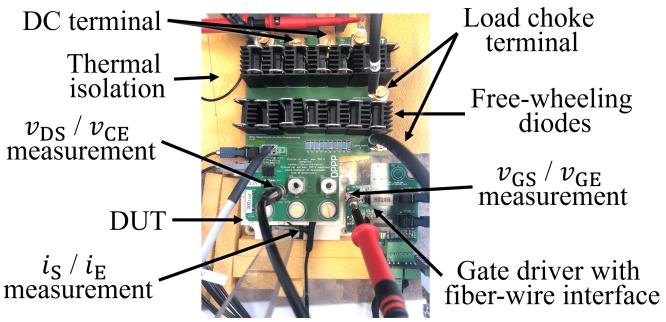

Fig. 8: Setup for output characteristic measurement at $T = -75°C$

The results for the *FF200R12KE4* Si-IGBT module are shown in Fig. 9. Due to its forward threshold voltage, especially for the IGBT, a measurement of the *I-V* curve at very low currents is of great interest. Hence, to increase the accuracy, two measurement curves are combined. Up to 15 A, the measurement is performed with $V_{DC} = 20\,V$. This results in smaller oscillations during the switching and a higher accuracy due to the smaller oscilloscope range. To enable current pulses up to 400 A, V_{DC} is increased to 200 V for currents greater than 15 A.

To calculate the *I-V* curve, first a moving average filter with a 50 element window width is applied to the signal. From the smoothed signal, 100 consecutive measured values are then averaged to form one *I-V* operating point.

For lower temperatures, the forward threshold voltages rises whereas the differential resistance falls, leading to a steeper characteristic. Hence, for the lower part-load operational range, lower static losses at higher junction temperatures occur, while for upper part-load and full-load the static losses decrease with lower temperatures. The temperature dependency of the forward voltage V_{CE} for $I_E = 30\,A$ in part-load operation and for the nominal current $I_E = 200\,A$ are given in Fig. 10.

At full-load operation the forward voltage can be reduced by around 20 % when operating the device at $-75°C$ compared to its conventional operation at

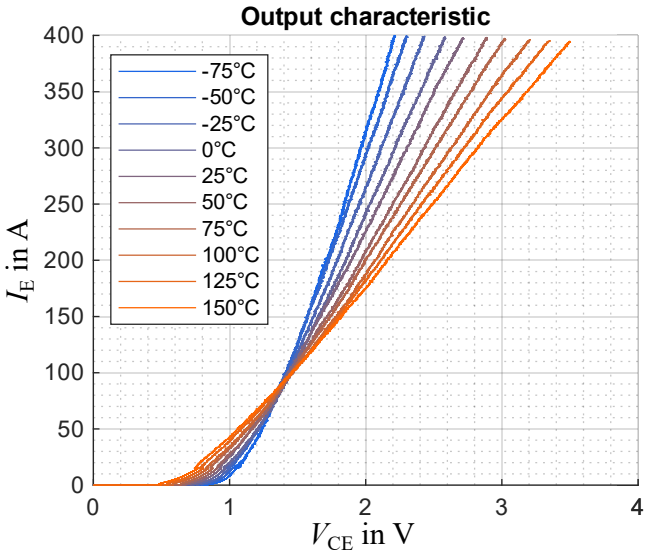

Fig. 9: *I-V* characteristic of the *FF200R12KE4* Si-IGBT module

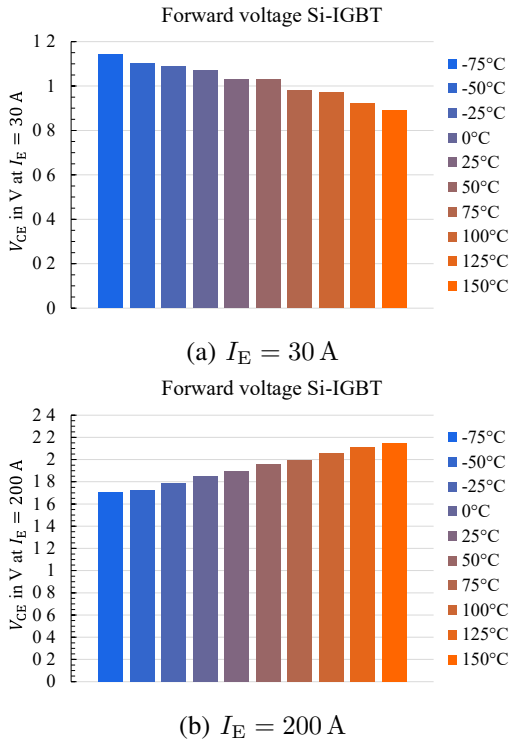

(a) $I_E = 30\,A$

(b) $I_E = 200\,A$

Fig. 10: V_{CE} of the *FF200R12KE4* Si-IGBT module over temperature

temperatures near the maximum junction temperature. For $I_E = 30\,A$ the lower temperature of $-75\,°C$ would result in an approximately 28 % higher forward voltage.

In the following, the results for the *FF6MR12KM1* SiC-MOSFET module are presented. Its output characteristic is shown in Fig. 11.

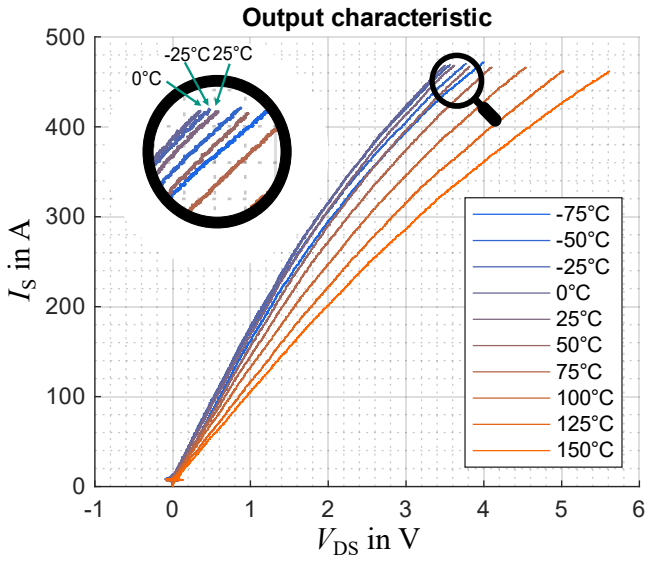

Fig. 11: *I-V* characteristic of the *FF6MR12KM1* SiC-MOSFET module

In contrast to the Si-IGBT module, all curves were recorded at $V_{DC} = 250\,V$. The small disturbances at very low currents result from the oscillation described in subsection V-B at the very beginning of the pulse and the lower accuracy due to the selected wider oscilloscope range.

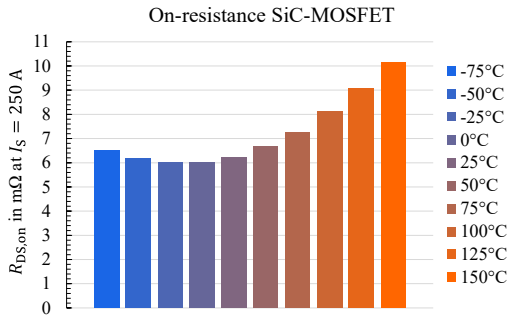

Fig. 12: On-resistance of the *FF6MR12KM1* SiC-MOSFET module for $I_S = 250\,A$ over temperature

The investigation of the the on-resistance at the modules nominal current $I_S = 250\,A$ is depicted in Fig. 12. It can be seen, that a minimum at around $-25 - 0°C$ occurs. For higher temperatures, a steep increase of the on-resistance can be observed, while for lower temperatures down to $-75°C$ the increase is moderate. When operating the module at $-25 - 0\,°C$, the on-resistance can be reduced by around $41\,\%$ compared to an operation at $150°C$, operating at $-75°C$ results in a reduction of approximately $36\,\%$.

D. Discussion

The measured output characteristics show good consistency with the values given in the data sheets [21] and [22] in a wide range. Differences at higher currents can be explained by the non-ideal load choke and the droop of the Rogowski coil which is not corrected yet. At the moment, the reason for the derivations at higher temperatures is not fully understood. A possible explanation could be the increase of the connectors contact resistance due to copper oxide formation at higher temperatures.

The temperature dependent semiconductor behavior known from literature is clearly visible in the measurements. For the Si-IGBT, as explained in [23, pp. 9-10, 34-35] the forward threshold voltage rises due to a lower intrinsic charge carrier density for lower temperatures. In contrast, the differential resistance falls, which can be explained according to [23, p. 101] by a higher carrier mobility. For the SiC MOSFET the temperature dependency of the on-resistance with its minimum at around $-25 - 0\,°C$ is in good consistency with the results presented in [9], [10], [15].

VI. Conclusion

Within this contribution, an easy-to-use, flexible, wide temperature range test bench for both static and dynamic characterization of power semiconductors was introduced. The operation over the full temperature range from -75 to $150°C$ was proven by dynamic characterization of a Si-IGBT module as well as static characterization of a Si-IGBT and SiC-MOSFET module. With minor adjustments, the static and dynamic measurement are performed with the same setup. Hence, no additional curve tracer is necessary. The results are in good consistence with previously published research, promising more efficient converters when their semiconductors are operated at lower temperatures.

Future work includes the adaption of the test bench to GaN semiconductors and the validation and characterization of further semiconductors at low temperatures. An extension for breakdown voltage measurements is also planned. The developed system represents a highly variable test bench for different semiconductor materials and module types, enabling the collection of the necessary information for a highly efficient low-temperature inverter design.

REFERENCES

[1] M. Saruwatari et al., "Design Study of 15-MW Fully Superconducting Generators for Offshore Wind Turbine," in IEEE Transactions on Applied Superconductivity, June 2016.

[2] H. -W. Cho et al., "Design and Preliminary Experiments of a Rotating Armature Partial Superconducting Air-Core Generator," in IEEE Transactions on Applied Superconductivity, Sept. 2022.

[3] M. K. Al-Mosawi et. al., "Construction of a 100 kVA high temperature superconducting synchronous generator," in IEEE Transactions on Applied Superconductivity, June 2005.

[4] Lengsfeld, S.; Sprunck, S.; Frank, S.R. et. al. "An Approach to the Design and the Interactions of a Fully Superconducting Synchronous Generator and Its Power Converter" in MDPI Energies, 2022

[5] M. Stemmle, F. Merschel, M. Noe, L. Hofmann and A. Hobl, "Superconducting MV cables to replace HV cables in urban area distribution grids," PES TandD pp. 1-5, Orlando, FL, USA, 2012

[6] A. Alekseev et al., "Wasserstoff-Verflüssigung, Speicherung, Transport und Anwendung von flüssigem Wasserstoff," 2023, doi: 10.5445/IR/1000155199.

[7] Gammon et. al. "The Cryogenic Testing and Characterisation of SiC Diodes," Materials Science Forum, 2014

[8] L. J. Woodend et al., "Cryogenic characterisation and modelling of commercial SiC MOSFETs," 2016 European Conference on Silicon Carbide and Related Materials (ECSCRM), Halkidiki, Greece, 2016

[9] K. Tian et al., "Characterization of 1.2 kV 4H-SiC power MOSFETs and Si IGBTs at Cryogenic and High Temperatures," 2017 14th China International Forum on Solid State Lighting: International Forum on Wide Bandgap Semiconductors China (SSLChina: IFWS), Beijing, China, 2017.

[10] J. Qi et al., "Dynamic Performance of 4H-SiC Power MOSFETs and Si IGBTs over Wide Temperature Range," 2018 IEEE Applied Power Electronics Conference and Exposition (APEC), San Antonio, TX, USA, 2018.

[11] H. Gui et al., "Characterization of 1.2 kV SiC Power MOSFETs at Cryogenic Temperatures," 2018 IEEE Energy Conversion Congress and Exposition (ECCE), Portland, OR, USA, 2018

[12] M. Mehrabankhomartash et al., "Static and Dynamic Characterization of 1200 V SiC MOSFETs at Room and Cryogenic Temperatures," IECON 2021 – 47th Annual Conference of the IEEE Industrial Electronics Society, Toronto, ON, Canada, 2021.

[13] J. Qi, et. al., "Dynamic Characterization of 1.2 kV SiC Power MOSFET Body Diode at Cryogenic and High Temperatures," 2018 1st Workshop on Wide Bandgap Power Devices and Applications in Asia (WiPDA Asia), Xi'an, China, 2018.

[14] H. Gui et al., "Review of Power Electronics Components at Cryogenic Temperatures," in IEEE Transactions on Power Electronics, May 2020

[15] R. Chen and F. Wang "SiC and GaN Devices with Cryogenic Cooling" in IEEE Open Journal of Power Electronics, 2021.

[16] F. Stamer "Prädiktive Gate-Ansteuerung zur Optimierung des Schaltverhaltens von IGBTs," Inst. of Electrical Engineering, KIT, Karlsruhe, Germany, 2021

[17] R. Schwendemann, et. al. "A Modular Converter- and Signal-Processing-Platform for Academic Research in the Field of Power Electronics," 2018 IPEC-Niigata 2018 -ECCE Asia, 2018

[18] IEC 60747-9:2019-11, Semiconductor devices - Part 9: Discrete devices - Insulated-gate bipolar transistors (IGBTs)

[19] IEC 60747-8:2010-12, Semiconductor devices - Discrete devices - Part 8: Field-effect transistors

[20] Z. Zhang, et. al., "Methodology for Wide Band-Gap Device Dynamic Characterization," in IEEE Transactions on Power Electronics, Dec. 2017

[21] Infineon "62mm C-series module with trench/fieldstop IGBT4 and Emitter Controlled diode" https://www.infineon.com/cms/en/product/power/igbt/igbt-modules/ff200r12ke4/ (accessed March 24, 2023), v3.0, November 2013

[22] Infineon "62mm C-Series module with CoolSiC Trench MOSFET", https://www.infineon.com/cms/en/product/power/mosfet/silicon-carbide/modules/ff6mr12km1/ (accessed March 24, 2023), v2.0, April 2020

[23] Josef Lutz, "Halbleiter-Leistungsbauelemente : Physik, Eigenschaften, Zuverlässigkeit,", Berlin, Germany, Springer Vieweg, 2012, ISBN:9783642297960